Part II
Mixing in Microsystems

6
Characterization of Mixing and Segregation in Homogeneous Flow Systems

Laurent Falk and Jean-Marc Commenge

6.1
Introduction

For more than 10 years, micromixers have demonstrated their capabilities in a wide range of applications, ranging from lab-on-a-chip biotech devices to industrial applications in replacing batch synthesis of a chemical to continuous reaction. Numerous examples can be found in textbooks [1] and in the chapters of the present handbook. Microfluidics, and especially mixing [2], are still a bubbling field with thousands of papers published and hundreds of patents issued each year [3, 4]. However, the design of micromixers is largely a trial-and-error process and new designs are driven by complex fabrication and fluid control techniques (such as microstereolithography and electro-osmosis). This situation may result in inefficiencies and suboptimal designs. Mixing issues are complicated and sometimes counterintuitive, because the results are issued from strongly coupled processes between fluid mechanics, mass transfer and reactions.

Mixing effects in chemical reactors are essentially related to the respective value of the characteristic times of mixing and reaction. If the reaction proceeds slowly compared with mixing, i.e. the mixing time is short with respect to the reaction time, the concentration field appears as totally homogeneous when reaction takes place. In that case, mixing has no further influence on the reactor performances. In contrast, if the reaction is fast compared with mixing, then mixing and reaction proceed simultaneously and not consecutively. Chemical reaction takes place in local zones, where mixing is realized. The medium behaves as a heterogeneous fluid, each region having its own apparent chemical rate. This may lead to a decrease in chemical conversion rate, and of yield and selectivity, inducing the formation of byproducts which have to be separated.

There exists a great variety of micromixers based on different mixing principles, classified in mainly two basic concepts (see Chapter 7):

- active mixers, which use external energy sources as mechanical stirrers and valves, piezoelectric vibrating membranes, ultrasound, acoustics;

Micro Process Engineering, Vol.1: Fundamentals, Operations and Catalysts
Edited by V. Hessel, A. Renken, J.C. Schouten, and J.-I. Yoshida

ISBN: 978-3-527-31550-5

- passive mixers, which use the flow energy to create multi-lamellae structures which are stretched and recombined to promote mixing by molecular diffusion.

A detailed list of these mixers, their mixing principles and operating conditions can be found in recent reviews by Nguyen and Wu [5], Squires and Quake [6] and more specifically by Hessel *et al.* [7] and in the next chapter of the present book. Almost every laboratory and company active in this field has proposed its own, or several, mixer(s). Because of the high number of mixers and of the lack of one standard performance quantification method, it is difficult for the user to compare and to choose between the different micromixers according to a specific purpose.

The present chapter aims to be complementary to the studies and reviews already published to present theoretical basis elements for the understanding of mixing principles in laminar flows, mainly developed in micromixers. Among different characterization techniques of mixing efficiency, this chapter more specifically focuses on the chemical test method, called the Villermaux–Dushman reaction, that we have developed over many years and which is named in memory of Professor Jacques Villermaux. It will be shown how to obtain the mixing time and how to relate it to operating parameters such as the Reynolds number of the flow and the specific power dissipation per unit mass of fluid. A non-exhaustive comparison of several micromixers will be presented.

6.2
Mixing Principles and Features of Microsystems

Consideration of length and time scales is fundamental as they provide an indication of the main mechanisms at work. The combination of length and time scales with material parameters such as molecular diffusivity and viscosity leads to dimensionless characteristic numbers that provide guides to the relative importance of competing mechanisms.

The Reynolds number, *Re*, is the ratio of inertial forces to viscous forces. If U and L denote the characteristic velocity and length scales, respectively, $Re = UL/\nu$, where ν is the kinematic viscosity. Small values of *Re* (i.e. less than 1000) correspond to laminar (viscosity-dominated) flows and large values of *Re* to turbulent flows.

The Schmidt number, $Sc = \nu/D$, is the ratio between two transport coefficients, where D is the molecular diffusion coefficient. *Sc* can be interpreted as the ratio of two rates. The rate at which concentration becomes smoothed out by molecular diffusion is proportional to $(Dt)^{1/2}$, where t denotes the time, whereas the rate for motion to spread out or die is proportional to $(\nu t)^{1/2}$. The ratio of these two rates is $Sc^{1/2}$. Thus, if $Sc \gg 1$, as in the case of liquids, concentration fluctuations survive without being erased by mechanical mixing until late in the process. The kinematic viscosity of water is about $10^{-6}\,m^2\,s^{-1}$. The diffusion coefficient of small molecules in water is about $10^{-9}\,m^2\,s^{-1}$; hence a typical value of *Sc* for a liquid such as water is about 1000.

The Peclet number, *Pe*, is the ratio of transport by advection (or convection) and by molecular diffusion; *Pe* is defined as $Pe = UL/D = ReSc$. *Pe* can be interpreted also as

the ratio of diffusional to advective time scales, where the time scale for diffusion is L^2/D and the time scale for convection is L/U. A large value of Pe indicates that advection dominates diffusion and a small Pe indicates that diffusion dominates advection, or, in terms of time scales, the fastest process dominates.

6.2.1 Molecular Diffusion

Molecular diffusion is the ultimate and finally the only process really able to mix components of a fluid on the molecular scale. The time constant for molecular diffusion is the diffusion time defined as

$$t_{\text{diff}} = A\frac{R^2}{D} \tag{6.1}$$

where R denotes the half-thickness of the aggregate and D the diffusion coefficient. A is a shape factor defined by

$$A = \frac{1}{(p+1)(p+3)}$$

where p is a shape parameter ($p=0$ for a slab, $p=1$ for a cylinder and $p=2$ for a sphere).

The aggregate then behaves approximately as a first-order dynamic system of time constant t_{diff} with respect to mass transfer. The choice of the characteristic dimension $l=2R$ depends on the kind of microstructure which is considered to exist when molecular diffusion becomes controlling. In complex real flow, the shape of the structures is of course impossible to define because of the multiple laminar vortices which deform the structures along the three dimensions of space. The previous relation of the shape factor, however, enables one to give an evaluation of the mixing time by simple diffusion.

Table 6.1 illustrates the order of magnitude of the diffusion time of a slab, considering the classical diffusion coefficient in water.

It can be noted that diffusion is a rather slow process and that mixing can be drastically enhanced by decreasing the size of the slab. The 50 µm scale can be considered as the lowest limit for industrial applications without any blocking problems or generating prohibitive pressure drops for high flow-rates. However, even at this small scale, the mixing time by diffusion is of the order of 1 s, which is far

Table 6.1 Order of magnitude of diffusion time of a slab in water ($D = 10^{-9}\,\text{m}^2\,\text{s}^{-1}$)

Size of the slab, R	Diffusion time
1 mm	5 min
500 µm	1.5 min
100 µm	3 s
50 µm	0.8 s

higher than the characteristic time of fast reactions of several milliseconds. To achieve such fast diffusion mixing, it would be necessary to handle slab sizes of only a few microns.

Mechanical energy is then required to reduce the initial size of the blob and create very fine structures which could further the effect of molecular diffusion. A turbulent flow field, three-dimensional and random, allows efficient stirring that is known to enhance mixing considerably and has been preferred for industrial applications, when possible. The price of this high efficiency is the large energy dissipation rate compared with laminar Stokes flows, but the latter require a longer time for full mixing. In small devices and microreactors, the characteristic size of the channels is of the order of several hundred microns. If one considers that flow regime laws are not changed in microstructures, which is probably the case according to Li *et al.* [8], flows are then almost laminar ($Re < 1000$) unless generating prohibitive pressure drops. In fact, as we will show below, laminar flow fields in microchannels can be very efficient for mixing.

6.2.2 Mixing in a Shear Field

Let us consider an aggregate which is subjected to a uniform flow with no velocity gradient (Figure 6.1a). All the points of the aggregate are convected with the same velocity and there is no deformation of the structure. In that case, the flow has no effect on mixing and the problem is brought back to the previous one of mixing by molecular diffusion.

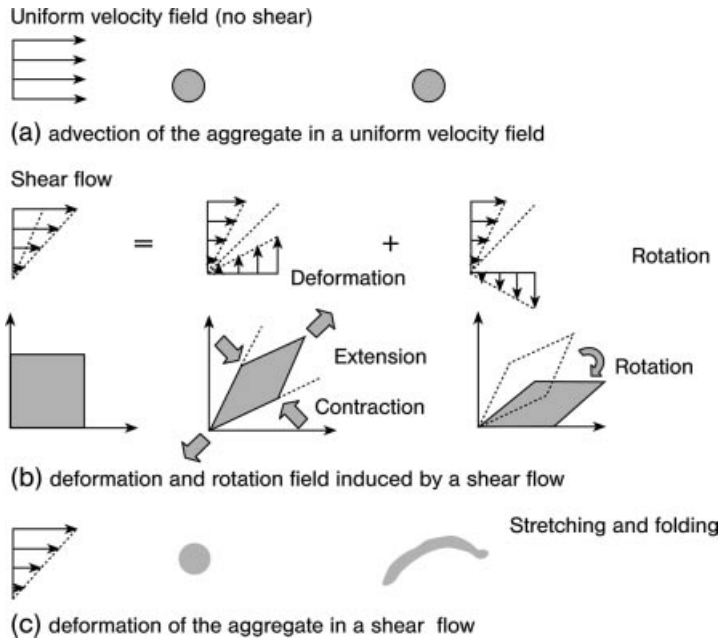

Figure 6.1 Deformation of lamellae in a uniform flow (a) and in a shear flow (b, c).

If this aggregate is now placed in a shear flow with a velocity gradient

$$\dot{\gamma} = \frac{du}{dz} = \sqrt{\frac{\varepsilon}{2\nu}}$$

where ε is the specific power dissipation in $W\,kg^{-1}$ of fluid, one can show (Figure 6.1b) that this flow can be decomposed into two additive parts called deformation and rotation fields. A fluid element will then be contracted and stretched by the deformation field and bent by the rotation field (Figure 6.1c).

The objective of mixing is to produce the maximum amount of interfacial area between two initially segregated fluids in the minimum amount of time or using the least amount of energy. Creation of interfacial area is connected to stretching of lines in two dimensions and the surface in three dimensions. A fluid element of length ℓ_0 at time zero has length $\ell(t)$ at time t; the length stretch is defined as $\lambda = \ell(t)/\ell_0$; if mixing is effective, λ increases nearly everywhere, although there can be regions of compression where $\lambda < 1$. In simple shear flow, the fastest rate of stretching, $d\lambda/dt$, corresponds to the instant when the element passes through the 45° orientation corresponding to the maximum direction of stretching in shear flow; for long times the stretching is linear ($\lambda \sim t$) in time as the element becomes aligned with the streamlines.

However, stretching also rapidly decreases the aggregate thickness, which may enhance diffusion mixing by increasing the concentration gradients. In a shear flow, the characteristic thickness δ of the blob is decreasing with time according to the following relation:

$$\frac{\delta(t)}{\delta_0} = \frac{1}{\sqrt{1 + (\dot{\gamma}t)^2}} \tag{6.2}$$

Let us consider the numerical application of the preceding relation to water flow in a microchannel of 500 μm diameter, with a mean velocity of 0.1 m s^{-1}. The maximum shear rate is estimated [see Equation (6.5) below] to be $\dot{\gamma} = 800\,s^{-1}$ The relative thickness (Figure 6.2) decreases very rapidly and in 10 ms the characteristic size of the lamellae is only 10% of its initial value.

It can be seen that, provided that the segregation scale is large (this notion will be clarified further), stretching is the controlling process for mixing and mechanical dissipation is an interesting tool to decrease the mixing time.

6.2.3
Application to Mixing in Microchannels

This section considers the case of flow in a channel of diameter d at low Re. After the flow has been in the pipe for a distance much longer than the entry length, the fluid velocity only varies with radial position. In the case of a cylindrical channel with flow along the axis, the velocity distribution is a simple quadratic, known as Hagen–Poiseuille or simply Poiseuille flow. The pressure drop is given by the following relation:

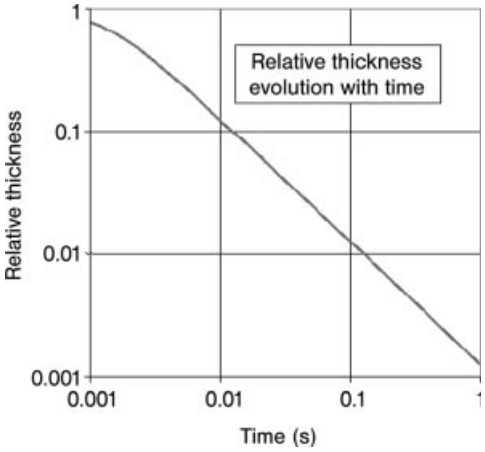

Figure 6.2 Time evolution of the relative thickness of a lamella in a shear flow (water, microchannel of 500 μm diameter, mean velocity = 0.1 m s^{-1}).

$$\frac{\Delta P}{L} = \frac{32\mu u_{\mathrm{m}}}{d^2} \tag{6.3}$$

where u_{m} is the mean velocity and ΔP is the pressure drop between two points separated by a length L.

The energy dissipation rate ε per unit mass of fluid (W kg^{-1}) is proportional to the product of the pressure drop and the flow rate:

$$\varepsilon = \frac{Q\Delta P}{\rho V} = \frac{32\nu u_m^2}{d^2} \tag{6.4}$$

where ν is the dynamic viscosity, Q the volume flow rate and V the volume of fluid between the two points of pressure drop measurement.

The mean shear rate in the tube can be easily calculated by

$$\dot{\gamma} = \left(\frac{\varepsilon}{2\nu}\right)^{1/2} \tag{6.5}$$

The shear flow induces a decrease in the characteristic dimension of the structure in the direction orthogonal to the elongation.

As illustrated in Figure 6.3, the molecular diffusion flux, which is inversely proportional to the aggregate thickness, may be strongly increased by stretching.

Diffusion and convection are then competitive processes, but according to the shear rate value, for large segregation scales, the diffusion process is slow compared with convection and mixing is almost controlled by stretching. At fine segregation scales, diffusion becomes the controlling step.

This problem has been analyzed by several groups [8–12] and reinvestigated by Baldyga and Bourne [12], who proposed to calculate the mixing time by the following relation:

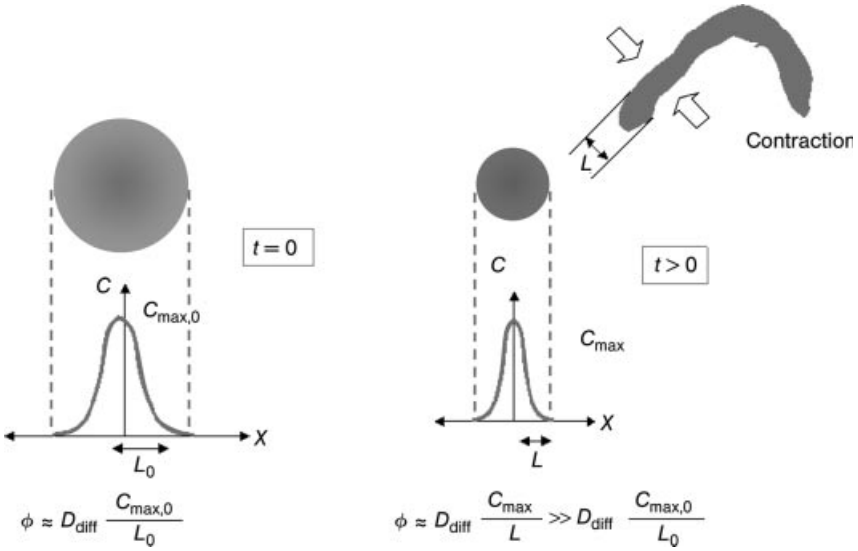

Figure 6.3 Diffusion enhancement in a shear flow.

$$t_{\text{diff}+\text{shear}} = \frac{\operatorname{arcsinh}}{2\dot{\gamma}}\left(\frac{0.76\dot{\gamma}\delta_0^2}{D}\right) \tag{6.6}$$

According to the expression for the shear in a tube with laminar flow and assuming that the initial striation thickness is equal to half of the channel diameter d, the mixing time is given by the flowing expression as a function of the Peclet number Pe:

$$t_{\text{diff}+\text{shear}} = \frac{d}{8\,\bar{u}}\operatorname{arcsinh}(0.76\ Pe) \tag{6.7}$$

In liquids, the Schmidt number is much higher than 1, of the order of 1000 in water. As a result, even at low flow velocity, the Peclet number is much higher than 1 (for a velocity of 1 mm s^{-1} in a channel of 100 µm diameter, $Pe = 100$). In this case, the arcsinh function can be simplified by a logarithmic function and the mixing time is given by

$$t_{\text{diff}+\text{shear}} = \frac{(d^2/D)}{8\ Pe}\ln(1.52\ Pe) \tag{6.8}$$

In Figure 6.4 is plotted the theoretical mixing time which could be obtained in microchannels of different diameters versus the Reynolds number, in the case of water. It can be seen that the mixing time decreases almost inversely proportionally with the Reynolds number. Potentially, the theoretical mixing time can be very small, much shorter than 1 ms in channels smaller than 1 mm in diameter and at $Re < 1000$.

The main interest in this relation is also to show the impact of size extrapolation of the channel upon the mixing time.

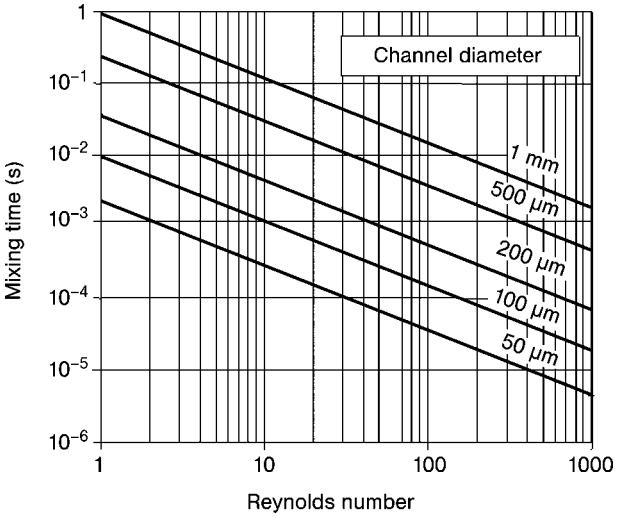

Figure 6.4 Theoretical mixing time versus Reynolds number in microchannels of different diameters (water, $Sc = 1000$).

The mixing time can also be expressed as a function of the power dissipation ε in a microchannel. According to the expression of the power dissipation in a channel in laminar flow,

$$\varepsilon = 32\,\nu\left(\frac{u}{d}\right)^2$$

the mixing time can be estimated by

$$t_{\mathrm{diff+shear}} = \frac{1}{\sqrt{2}}\left(\frac{\nu}{\varepsilon}\right)^{1/2}\ln(1.52\,Pe) \tag{6.9}$$

Owing to the smoothing effect of the logarithmic function, this relation shows that the mixing time becomes practically independent of the Peclet number, and therefore of the channel diameter, as can be seen in Figure 6.5. It can be observed that, potentially, very low values of mixing times, far below 1 ms, can be reached.

6.2.4 Chaotic Mixers

Numerous micromixers have been designed based on the principle of laminar static mixers, where the fluid undergoes a periodic process of splitting, rotation and recombining. These mixers are inspired by chaotic mixing, where the geometry of the system imposes spatial periodicity.

Chaotic motion generated by periodic flow represents an important class of chaotic flows in general. Chaotic mixing is characterized by an exponential rate of stretching (as opposed to linear stretching in a non-chaotic flow) of fluid elements. As a fluid

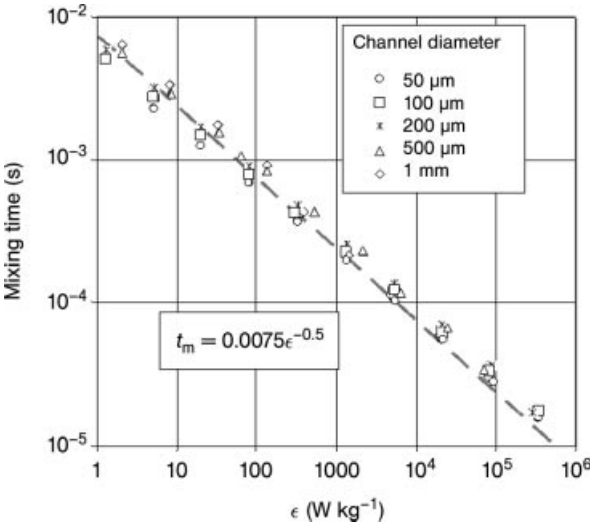

Figure 6.5 Theoretical mixing time versus specific power dissipation in microchannels of different diameters (water, $Sc = 1000$).

element travels through a chaotic flow, it is not only stretched, but also reoriented due to the repeated change in the direction of the flow field that acts on it. Reorientation leads to folding of material area exponentially and reduces correspondingly the scale of segregation of the system, also at an exponential rate, following a general iterative "horseshoe" or "baker's transformation" mechanism.

As presented above, a mixing time relation can be derived for chaotic mixing in microchannels [14, 15]. Using a simple representative model [18, 22], presented hereafter in additional readings, it is possible to show that the mixing time can be given by the following general relation:

$$t_{\text{chaotic}} \sim \frac{d^2}{\nu}\frac{1}{Re}Pe^b \tag{6.10}$$

where d denotes the channel diameter and b is an exponent which ranges from 1 (pure diffusion, $Pe < 1$) to 0 ($Pe \gg 1$) according to Figure 6.6.

Giona *et al.* [19] have shown that a wide class of unidirectional flows in periodic domains give a convection-enhanced diffusion with $b = 1/2$.

In fact, it is difficult to generate homogeneous flows where shear rate is constant in the domain and, in chaotic flows, the striation pattern quickly develops into a time-evolving complex morphology of poorly mixed regions of fluid (islands) and of well-mixed regions. Islands translate, stretch and contract periodically and undergo a net rotation, preserving their identity on returning to their original locations. Stretching within islands, on average, grows much less than in chaotic regions. Moreover, since islands do not exchange matter with the rest of the fluid, they represent an obstacle to efficient mixing.

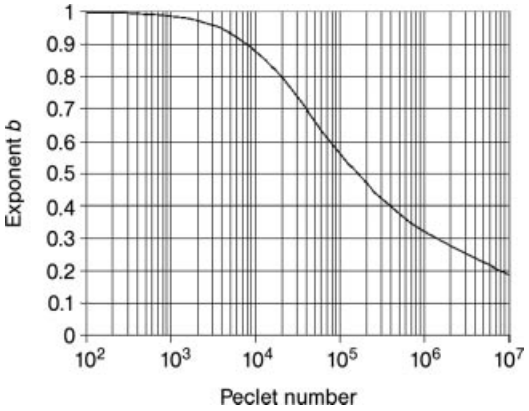

Figure 6.6 Theoretical value of the exponent b versus the Peclet number [power-law mixing time Equation (6.10) for chaotic mixing].

Several authors have shown that in laminar flows, mixing time scales as a power law of the Peclet number. Thus, Meunier and Villermaux [20], Gleeson [21] and Raynal and Gence [22] showed that in some regions $t_{\text{chaotic}} \sim Pe^{1/3}$, but in other cases $t_{\text{chaotic}} \sim Pe^{1/5}$ and in pure chaotic flows $t_{\text{chaotic}} \sim Pe^{1/2}\ln Pe$ (similar to $t_{\text{chaotic}} \sim Pe^{1/3}$).

In laminar flows with several vortices, Gerlinger *et al.* [23] showed the importance of the initial concentration field for the mixing rate and proposed a general power-law $t_{\text{mix}} \sim Pe^{b}$ with b between 1 and 0.3.

As will be shown later, the general Equation (6.10) allows the representation of all types of laminar mixers, even those which show no fully chaotic behavior. This can be explained by the fact that any real complex flow presents a mechanism of material stretching, reorientation and folding which is more or less repeated along the flow.

For $Pe \gg 1$, Equation (6.10) becomes:

$$t_{\text{chaotic}} \sim a\frac{d^2}{\nu}\ln Pe$$

where the mixing time is found to scale as $\ln Pe$, which is in agreement with Equation (6.8) in pure shear flow. This result is classical and was already known to Ott and Antonsen [24], Raynal and Gence [25] and Wiggins and Ottino [2] and Stroock *et al.* [17].

For low Pe, the general Equation (6.10) can be simplified and it can be checked that the expression leads to the limit case for pure diffusion:

$$t_{\text{chaotic}} \simeq \frac{d^2}{\nu}Pe = \frac{d^2}{D}$$

6.2.4.1 **Additional Readings: Chaotic Mixing Model in Microchannels** [18, 22]

Let us consider that for one cycle of chaotic advection, a fluid particle attached to a lamella travels a distance $\ell = \alpha d$, proportional to the diameter d of the channel, where α is a proportionality factor.

After n cycles have been completed, the lamella has been advected over a distance $n\ell$ and the time for transport by convection is simply estimated by

$$t_{\text{conv}} = \frac{n\ell}{u} = n\left(\frac{\alpha d}{u}\right)$$

For each cycle of chaotic advection, the striation thickness of the lamella decreases by a factor f. If the initial striation thickness is approximately equal to the diameter d of the microchannel, the striation thickness δ for later positions is determined by

$$\delta = d(f)^{-n}$$

where n is the number of fold, stretch and reorient cycles.

The classical expression for the striation thickness evolution with time, $\delta = \delta_0 \exp(-\lambda t)$, where λ is the Lyapounov exponent, shows that f and n values are related to λ.

Combining the mixing time by pure diffusion [Equation 6.1] and the striation thickness relations, the time-scale for mixing by diffusion after n cycles is then

$$t_{\text{diff}} = A\frac{\delta^2}{D} = A\frac{d^2(f)^{-2n}}{D}$$

Following Stroock *et al.*'s assumption [17], the mixing time in chaotic flow, t_{chaotic}, is approximately the time when the times for convective transport and diffusive mixing are matched. This means that the mixing time is assumed to be approximately equal to the residence time, after which the diffusion time over the striation thickness is equal to or smaller than the already elapsed residence time:

$$t_{\text{diff}} = t_{\text{conv}}$$

After rearrangement, one obtains the expression for the Peclet number of the flow:

$$Pe = \frac{ud}{D} = \frac{\alpha}{A} n(f)^{2n}$$

By taking the logarithm of both sides of the equation:

$$\ln Pe = \ln\left(\frac{\alpha}{A} n\right) + 2n \ln f$$

the expression can be simplified in two cases according to the value of the Peclet number.

- For large Pe, one can show that $\ln n \ll 2n \ln f$ and $n \sim \ln Pe$. By replacing the derived value of n in the equation for transport by convection, the mixing time is defined by

$$t_{\text{chaotic}} \sim \alpha \frac{d}{u} \ln Pe \sim \alpha \frac{d^2/D}{Pe} \ln Pe$$

- For very low Pe, n is almost proportional to Pe, $n \sim Pe$, and the mixing time becomes

$$t_{\text{chaotic}} \sim \frac{d^2}{\nu} Sc = \frac{d^2}{D}$$

which is in fact the limit case for pure diffusion.

The general solution of the problem is difficult to find because it requires the knowledge of parameters α, A and f. The determination of the values is extremely difficult because the flowing fluid undergoes periodic cycles which are neither constant nor equivalent in a real mixer.

Likewise, the value of the proportionality factor α and the Lyapounov exponent (which can be shown to be proportional to the mean velocity gradient [22]) may change along the flow.

Moreover, the diffusion model assumes a blob geometry which is not in reality a simple slab, a cylinder or a sphere but a complex 3D structure for which the shape factor A is not known. One can, however, present a general power-law where $n \sim Pe^b$, where the power b varies according to the Peclet number. In that case, the mixing time can be given by Equation (6.10).

6.2.5
Mixing Efficiency

We have shown that the theoretical mixing time in microdevices can be very small. Theses values have been obtained, however, in a perfect situation which is not encountered in reality. Several main objections can be raised.

First, the mixing time considers an initial concentration field constituted of interlaced slabs of components A and B. In fact, this state is not instantaneously realized at the mixer inlet and additional time is required to mix the two flows in order to obtain a sandwich structure with n intertwined lamellae.

Second, it has been assumed that the lamellae are continuously submitted to a constant shear rate. In reality, because of the complex three-dimensional flow field, the lamellae are rotated and do not undergo a constant deformation rate.

Another objection concerns the orientation of the deformation field. It may happen that a lamella is perpendicular to the stretching field and in that case the striation thickness increases, which induces the reduction of the concentration gradient and slows the mixing rate.

Finally, it is common that the flow field and the concentration field do not match. Mechanical energy is used to achieve the flow in the device, but in zones of pure component A with no interface with another component B, this mechanical energy does not contribute to mixing.

All theses considerations mean that part of the consumed mechanical energy is used for mixing. Ottino *et al.* [26] proposed to introduce the concept of energetic efficiency of mixing, defined by

$$\eta = \frac{\dot{\gamma}}{\dot{\gamma}_{max}} = \frac{\dot{\gamma}}{\sqrt{\varepsilon/(2\nu)}} \tag{6.11}$$

where $\dot{\gamma}$ represents the shear rate which is effectively used for mixing and $\dot{\gamma}_{max}$ is the total shear rate used for the flow. It is impossible to determine theoretically the value of the energetic efficiency of mixing, but we will show below how it is possible to determine it from experimental data. Baldyga *et al.* [27] have shown that the value is very low, however, less than 1%, in twin-screw extruders.

Equation (6.8), giving the mixing time with respect to the shear rate, can be easily corrected to consider the energetic efficiency η. The mixing time is then given by

$$t_{\mathrm{diff+shear}} = \frac{d}{8\bar{u}}\eta \ln(1.52\, Pe\, \eta) \tag{6.12}$$

In laminar liquid mixing applications, the range of variation of the Peclet number is between 10^3 and 10^6. Assuming an energetic efficiency η of several percent, $Pe\,\eta \gg 1$ and the mixing time can be estimated by the following relation:

$$t_{\mathrm{diff+shear}} \sim \frac{d}{\bar{u}} Pe^{0.15}\, \eta^{-0.85} \tag{6.13}$$

This expression shows that the mixing time is in practice almost inversely proportional to the mixing efficiency. For predetermined channel size and fluid velocity, the design of the internal structure of a micromixer is then primordial to maximize the mixing efficiency, i.e. to minimize the mixing time.

6.3 Experimental Mixing Characterization

Experimental characterization of the mixing quality in conventional stirred tank reactors, as well as in micromixers, is an important step for the proper comprehension of the performance of chemical reactors. To identify interactions between mixing and chemical reactions and quantify them, a variety of physical and chemical methods have been developed, whose application to a given mixer may either be easy or may require appropriate adaptations to obtain valuable measurements. The next section gives a brief overview of existing methods.

6.3.1 Physical Methods

Let us consider an imperfect mixture in which the concentration C of a given component is not uniform and let $p(C)$ be the local concentration distribution such that $p(C)\mathrm{d}C$ is the volume fraction of the mixture where the concentration is comprised between C and $C + \mathrm{d}C$. The average concentration is

$$\langle C \rangle = \int_0^{C_{\max}} C p(C) \mathrm{d}C \tag{6.14}$$

and the variance distribution is

$$\sigma^2 = \int_0^{C_{\max}} (C - \langle C \rangle)^2 p(C) \mathrm{d}C \tag{6.15}$$

Several indices may be defined to characterize the quality of mixing [28], including the classical "intensity of segregation", I_s ($\sqrt{I_s}$ is also used):

$$I_s = \frac{\sigma^2}{\sigma_0^2} \tag{6.16}$$

where $\sigma_0^2 = \langle C\rangle(C_o - \langle C_o\rangle)$ is the variance at the initial conditions before mixing.

Mixing time may be defined as the time required for I_s to fall to some prescribed fraction of their values before complete mixing. In Lagrangian coordinates, a characteristic time constant is defined by

$$t_{\text{mixing}} = -\frac{\sigma^2}{(d\sigma^2/dt)} \tag{6.17}$$

The size of segregated regions is characterized by the scale of segregation, defined from the autocorrelation function as:

$$\lambda_s = \int_0^\infty \frac{\langle c(x)c(x+r)\rangle}{\sigma^2}\, dr \tag{6.18}$$

where $c = C - \langle C\rangle$at position x and r denotes the distance between two points.

Physical methods then consist in measuring the segregation (i.e. variance) decay of a tracer along the flow in the mixer. Knowing the internal velocity field, it is then possible to transpose position and time to estimate the mixing time [29, 30].

In spite of the diversity of mixing indices, it clearly appears that the value of the degree of mixing measured experimentally will depend on the spatial resolution of the probe used to estimate local concentrations C in the mixture. Depending on the kind of application, a decrease in the length scales on which these variations are present or reductions in their amplitudes – or both – are desired. Although it may be sufficient to diminish the scale at which segregation persists below some moderate value to obtain the desired product quality in the case of the production of blends, mixing on the molecular level is necessary for any chemical reaction to occur.

The physical methods developed to determine mixing quality are mainly based on contacting one transparent liquid stream with a dyed liquid stream [31–33]. Visualization of the dye spreading along the channel of a continuous mixer using a microscope or a camera gives information about the mixing quality by following the segregation decrease. Unfortunately, since visualization is conducted perpendicularly to the flow, the imaging analysis only gives an average value of the dye concentration over the mixer depth. As a result, a visually-uniform dye concentration may either be interpreted as a complete mixing or as a regular multi-lamellae flow of various concentrations. In addition to this intrinsic uncertainty, these methods require transparent devices, which may be difficult to realize for complex geometries or operating conditions.

Variations of this method include the use of a fluorescent dye such as fluorescein or Rhodamine. Depending on the visualization technique used, the uncertainty between perfect mixing and multi-lamellae flow may still be detrimental to proper quantification of the mixing quality. Nevertheless, the use of confocal scanning microscopy enables one to perform three-dimensional imaging of the flow and distinguish between these configurations [17, 34, 38].

As explained, the main drawback of passive tracer (physical) methods arises if the sampling volume is larger than the smallest segregation scales. Under these circumstances, it is impossible to determine whether the two fluids are mixed or not within the measurement resolution. Several authors [39] have pointed out that the problem of finite sampling volume can be solved by using a fast and irreversible chemical reaction of the type $A + B \rightarrow P$. If dilute reactant is added to one stream and B to the other, then the amount of chemical product formed is equal to the amount of molecular scale mixing between the two streams at the reaction stoichiometric ratio. This is the reason why chemical methods have been developed.

6.3.2 Chemical Methods

The first mixing characterization methods using a chemical method were proposed in the early 1960s. The simple principle is based on the fact that when the mixing characteristic time and reaction characteristic time are of the same order of magnitude, the two processes are competing. The consumption rate of the reactants is then lower than the intrinsic chemical rate and, thanks to a model describing the coupled reaction and mixing processes, it is possible to determine the mixing time.

Different types of chemical systems can be used to monitor mixing quality in continuous mixers. The most elementary setup consists in contacting acidic and basic streams containing a pH indicator, such as phenolphthalein or Bromothymol Blue. The color change along the channel gives information on the fluid segregation [40–44]. Unfortunately, only qualitative information can be obtained due to the visualization mode and additional non-linear color changes. More precise information can be obtained using reactions that yield a colored product [31, 45, 46].

The use of a single reaction requires the online measurement of the local species concentration along the flow. With such systems, one experiences the main drawback of physical methods with the local measurement and the influence of the probe size on the mixing quality estimation. For that reason, the so-called test reactions are very attractive. Two main systems, based on competitive chemical reactions, have been proposed for the investigation of mixing effects, that is, the competitive consecutive reaction system (Scheme 6.1) and the competitive parallel reaction system (Scheme 6.2). Let us consider the following simplest reactions schemes which do not exactly match the published real systems, but which facilitate the comparison:

$$\mathrm{A} + \mathrm{B} \rightarrow \mathrm{R} \qquad (\mathrm{R1})$$

$$\mathrm{R} + \mathrm{B} \rightarrow \mathrm{S} \qquad (\mathrm{R2})$$

Scheme 6.1

$$\mathrm{A} + \mathrm{B} \rightarrow \mathrm{R} \qquad (\mathrm{R1})$$

$$\mathrm{C} + \mathrm{B} \rightarrow \mathrm{S} \qquad (\mathrm{R2})$$

Scheme 6.2

The first reaction (R1) is very fast, almost instantaneous, and the second (R2) has a characteristic reaction time almost equal to the mixing time which has to be measured. The procedure consists in adding reactant B in stoichiometric defect to A (Scheme 6.1) or to a premixture of A and C (Scheme 6.2).When aggregates of B are very rapidly mixed (much faster than the second reaction can proceed), species B is totally consumed by the first reaction and no product S is formed. In contrast, if mixing is slow, there is a local over-concentration of B compared with A and the formation of species S is possible. The higher the concentration of S, the lower is the mixer efficiency. The main advantage of these test-reactions is the record of mixing processes from the entry to the outlet of the mixer and the fact they do not require the local measurement of concentrations along the flow. A simple sampling at the mixer outlet is sufficient.

Two experimental methods have been used to characterize micromixer efficiency such as in the reaction of 1-naphthol and 2-naphthol with diazotized sulfanilic acid [47], but the most commonly used system such as the iodide–iodate reaction also called the Villermaux–Dushman reaction [48]. These test-reactions have in common that they generate a product whose selectivity is mixing sensitive, since this selectivity depends on the competition between mixing effects, that depend only on hydrodynamic conditions and the reaction rates, which depend on the reactant concentrations. As a consequence, for a given mixing time (e.g. at fixed flow rate through a given mixer), various selectivities are measured for various reactant concentrations, due to the change in the reaction time with respect to the fixed mixing time. This difficulty, related to operating conditions and experimental protocols, therefore requires that particular attention is paid to the analysis of the results obtained with these methods, particularly when different protocols are used. To avoid these problems, the next section presents the main steps of the methodology enabling one to extract the intrinsic mixing time from the experimental results, using the Villermaux–Dushman reaction as an example.

6.3.3
Villermaux–Dushman Reaction

The iodide–iodate test reaction is based on a system of two competing parallel reactions [48]:

$$H_2BO_3^- + H^+ \rightleftharpoons H_3BO_3 \qquad \text{quasi-instantaneous} \qquad \text{(i)}$$

$$5I^- + IO_3^- + 6H^+ \rightleftharpoons 3I_2 + 3H_2O \quad \text{very fast} \qquad \text{(ii)}$$

Whereas the reaction rate of the neutralization reaction (i) can be considered infinitely fast, the rate of the redox reaction (ii) is "only" fast and in the same range of rate as the micromixing process. The kinetics of reaction (ii) has been determined experimentally and can be written as

$$r = k[H^+]^2[I^-]^2[IO_3^-]$$

where k denotes the kinetic constant, which is a function of the ionic strength.

In addition to these reactions, the iodine formed by reaction (ii) can further react with iodide ions I^- to yield I_3^- ions according to the quasi-instantaneous equilibrium

$$I_2 + I^- \rightleftharpoons I_3^- \qquad \text{(iii)}$$

In practice, I_3^- is the key species whose concentration can be easily monitored by spectrophotometry with UV light at a wavelength of 353 nm [48]. To perform these measurements, the test procedure consists in injecting in stoichiometric defect a flow rate of sulfuric acid into a mixture of iodate, iodide and borate ions. Under perfect mixing conditions, the injected acid is instantaneously dispersed in the reactive medium and consumed by borate ions according to the neutralization reaction (i), which is infinitely faster than redox reaction (ii). In the opposite situation, when the mixing time of the acid with borate is in the same range or larger than the characteristic reaction time of the redox reaction (ii), there is a local over-concentration of acid which after complete consumption of $H_2BO_3^-$ can react with iodide and iodate surrounding ions to yield iodine. The selectivity of iodine, which can be deduced from the measurement of I_3^- concentration is then a measure of segregation state of the fluid.

As indicated above, these values of selectivities give preliminary information concerning the mixing quality, but such a selectivity comparison requires the use of similar protocols in a given mixer. Moreover, several difficulties are associated with this test reaction and must be checked before proper analysis of the results. First, the use of hydrochloric acid instead of sulfuric acid is prohibited because the chloride ions may react with the iodine ions and change the species equilibrium. In addition, the twofold role of borate ions must be considered. Indeed, borate ions not only are reactants of the neutralization reaction (i) but also play the role of buffer to maintain the solution pH constant. This pH value is judiciously chosen with respect to the potential–pH diagram of the water–iodine system, which gives the value of the iodine dismutation pH (pH^*) as a function of total iodine element concentration [49]. Under conditions favoring segregation in the vicinity of acid aggregates, local zones of pH lower than pH^* may appear, where the formation of iodine is thermodynamically possible. As these aggregates are progressively dissipated by shear and diffusion and H^+ ions are consumed, the local pH in these zones increases to reach its final value equal to the mean value of the overall solution. If the mean pH value is lower than pH^*, iodine is naturally formed even in the absence of acid aggregates. This is due to the reaction between iodide and iodate with H^+ released by $H_2BO_3^-/H_3BO_3$ buffer for which equilibrium is shifted to the left. In order to detect the presence of acid aggregates due only to bad mixing, the average working pH must be greater than pH^*. However, at strongly basic pH much larger than pH^*, the formed iodine is thermodynamically unstable and its dissociation can be non-negligible. In order to prevent this effect, the average working pH must be closer as possible to pH^*.

If the operating conditions are properly defined to prevent these difficulties, the measured I_3^- concentrations can be used to quantify in an explicit way the mixing quality. The results are first used to calculate the segregation index X_S, which is related to the concentration of iodine formed. The value of this index X_S lies between

0 and 1, where $X_S = 0$ denotes perfect mixing whereas $X_S = 1$ denotes total segregation conditions. The segregation index X_S is defined as

$$X_S = \frac{Y}{Y_{ST}} \tag{6.19}$$

where

$$Y = \frac{2([I_2] + [I_3^-])}{a[H^+]_0}$$

and

$$Y_{ST} = \frac{6[IO_3^-]_0}{[H_2BO_3^-]_0 + 6[IO_3^-]_0}$$

where Y denotes the ratio of the quantity of acid consumed by reaction (ii) to the total quantity of injected acid, Y_{ST} is the value of Y under total segregation conditions (infinitely slow mixing) and a the ratio of the acid flow rate to the borate–iodide–iodate flow rate. Under segregation conditions, both reactions (i) and (ii) appear instantaneous with respect to the mixing rate and the acid consumption is related to concentrations of borate and iodide–iodate ions. The intermediate calculation of iodine concentration can be found in [48].

For a double-jet system, acid solution and borate–iodate–iodide ions solution are fed separately in the two jets. This kind of system generally uses equal flow rates for the two feeds. The concentration in each feed must be adjusted to the ratio of the volume flow rates of the feeds. A rule which can be given in a first approach is that the ratio of the molar flow rates of the reactants have to be the same as the molar numbers ratio in a batch system:

We can propose the following procedure for continuous micromixers:

$$(I_{2\ \text{potential}}) = 3(IO_3^-)_0 = \frac{3}{5}(I^-)_0 = 2.1 \times 10^{-3}\ \text{M}$$

$$\left.\begin{array}{l}(H_3BO_3)_0 = 0.5\ \text{M} \\ (NaOH)_0 = 0.25\ \text{M}\end{array}\right\} (H_2BO_3^-) = 0.25\ \text{M}$$

$$(H^+)_0 = 0.117\ \text{M}$$

However, the concentrations set used for results presented in Figure 6.6 is also suitable.

As mentioned above, the segregation index is a measure of the influence of hydrodynamics on chemical selectivity. It depends on two phenomena:

- the chemical reactions with characteristic times t_{r1} and t_{r2}, which are directly related to the kinetics of reactions (i) and (ii)
- the physical process of mixing with the mixing time t_m, which is mainly a consequence of the hydrodynamics.

For constant initial reactant concentrations, which imply constant values of t_{r1} and t_{r2}, the variation of X_S accurately accounts for the variation of t_m. In practice, it can

effectively be observed that improvement of mixing conditions induces a decrease in the segregation index. Unfortunately, if non-constant mixing time and reaction time conditions are used, interpretation of the results is more complex. Chemical test reactions have been carried out to characterize mixer efficiency. If relative mixer comparison is possible and relevant, it is impossible, however, simply from the absolute value of the segregation index to predict the selectivity which will be obtained with another chemical system used for real applications (organic synthesis, polymerization, etc.). To obtain such information, a specific mixing model, based on mixing and reaction coupled processes, is required.

6.3.4
Mixing Time

Mixing time determination should require a complete model with full description of velocity and concentration fields in the mixer. This is the difficult task of reactive flow simulation that would necessitate the description of transport, stretching and diffusion coupled with reaction of very fine structures down to the Batchelor scale of about several microns.

In order to overcome this difficulty, many phenomenological models [50–54] have been proposed to describe mixing phenomena. A simple one, the IEM model (Interaction by Exchange with the Mean) [53, 54], assumes that the acid-rich zone exchanges mass with a borate-rich zone with a characteristic time constant, which is the mixing time. The objective of such a model is to deliver the order of magnitude of mixing time for practical applications and not to propose properly a detailed description of mixing phenomena.

If the internal flow in a micromixer can be described by a plug flow, it follows that there is no backmixing and that each acid-rich aggregate is in interaction with an iodate–iodide-rich aggregate of the same age. In this condition, the IEM model takes a simple formalism to represent the interaction of the two reactant flows.

The acid flow rate has a volume fraction of the total flow rate α and then the other inlet composed of iodide–iodate–borate mixture has a volume fraction $1-\alpha$.

For each chemical species, there are two differential equations, one for each stream (where the subscript 1 denotes the acid-rich stream and subscript 2 the iodide–iodate-rich stream).

$$\begin{cases} \dfrac{dC_{k,1}}{dt} = \dfrac{<C_k> - C_{k,1}}{t_\mu} + R_{k,1} \\ \dfrac{dC_{k,2}}{dt} = \dfrac{<C_k> - C_{k,2}}{t_\mu} + R_{k,2} \\ <C_k> = \alpha C_{k,1} - (1-\alpha) C_{k,2} \end{cases} \tag{6.20}$$

where $C_{k,1}$ and $C_{k,2}$ are the concentrations of species k in streams 1 and 2, respectively, $<C_k>$ is the mean concentration of k and $R_{k,1}$ and $R_{k,2}$ are the reaction rates for species k in streams 1 and 2, respectively.

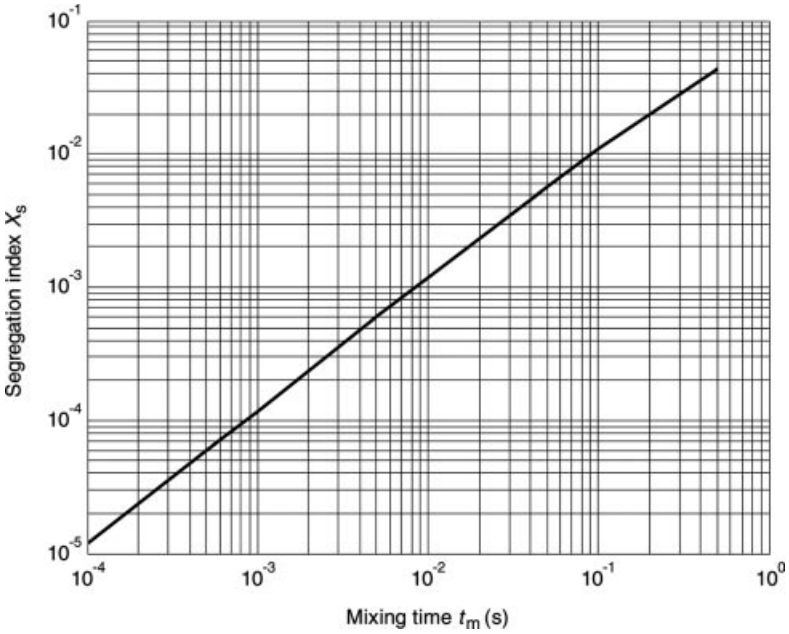

Figure 6.7 Evolution of the segregation index X_S with respect to the mixing time t_m for the following concentrations set: $C(KI) = 0.0319\ mol\ L^{-1}$, $C(KIO_3) = 0.00635\ mol\ L^{-1}$, $C(NaOH) = 0.0898\ mol\ L^{-1}$, $C(H_3BO_3) = 0.0898\ mol\ L^{-1}$ and $C(H_2SO_4) = 0.015\ mol\ L^{-1}$.

These equations give the time evolution of species in each stream by a reversible exchange between segregated regions and their mean environment through a single time constant t_μ and by reaction.

To relate the mixing time and the segregation index, one first assumes a value of the mixing time and solves the system of equations. At total conversion of acid, one obtains the final values of the iodine and triiodide concentrations, which allow the calculation of the segregation index X_S. The procedure is then repeated for a new value of the mixing time. All the couples (segregation index, mixing time) are then plotted to obtain the curve giving the mixing time as a function of segregation index (Figure 6.7).

6.4 Comparison of Performances of Micromixers

There are numerous experimental studies on micromixer characterization and, among the different methods, the well-known Villermaux–Dushman reaction is one of the most used. A few papers have proposed the comparison of the mixers performances thanks to these chemical reactions. As explained previously, mixing quality is a relative concept with regard to chemical reaction and chemical test methods

are very sensitive to the set of species concentrations which is used in the procedure. With a set of low concentrations, the reaction rate in competition with the mixing process is low and the mixing quality appears good. For the same hydrodynamics conditions, by using a high concentration set, the mixing quality appears as poorer.

Many authors have adapted their own concentration protocol of the Villermaux–Dushman method so that it is almost impossible to compare the performances of the studied micromixers simply by the confrontation of the segregation indices. The best way to propose a comparative study is to consider mixing times which are independent of the chemical conditions. Below we present a detailed comparison of the mixing times in different mixers. The theoretical developments presented previously are used to propose an interpretation of experimental data versus the Reynolds number and the power dissipation. From the confrontation with theoretical values, the energetic mixing efficiency in micromixers can be estimated.

Several studies have been considered, particularly those with no experimental errors in the use of the Villermaux–Dushman reaction protocol and with providing important information such as mixer geometry (channel sizes, internal volume), flow rate and pressure drop. The following studies have been analyzed:

1. Panic *et al.* [55], who compared five types of micromixers: the accoMix micromixer from Accoris based on the split-and-recombine principle, the standard slit interdigital micromixer from IMM based on the multilamination principle, the triangular interdigital micromixer from Mikroglas based on the multilamination principle, the caterpillar micromixer from IMM based on the split-and-recombine principle and a T-mixer from Bohlender.
2. Kockmann *et al.* [56], who studied the mixing in T-mixers with rectangular cross-sections of different sizes and aspect ratios, with: width of the mixing channel $\times$ width of the entrance channel $\times$ depth of the channels in micrometers of ($600 \times 300 \times 300$), ($400 \times 200 \times 200$) and ($200 \times 100 \times 200$). They also studied several single mixing elements arranged in parallel, a T-tree mixer, a tangential mixer and a T-cascade mixer.
3. Nagasawa *et al.* [57], who studied the K-M mixers based on collision principle in a star or a snowflake geometry. Four geometries have been investigated (number of channels n, channel width W, diameter of the mixing zone D: $n1 = 14$, $W1 = 50\,\mu m$, $D1 = 220\,\mu m$; $n2 = 10$, $W2 = 100\,\mu m$, $D2 = 320\,\mu m$; $n3 = 8\,\mu m$, $W3 = 200\,\mu m$, $D3 = 520\,\mu m$; $n4 = 8$, $W4 = 200\,\mu m$, $D4 = 220\,\mu m$ with specific injection zone).
4. Keoschkerjan *et al.* [58], who investigated the performance the FAMOS toolkit integrating a micromixer based on the multilamination principle.
5. Schneider *et al.* [59], who studied a Y-micromixer with a 90° angle.
6. Men *et al.* [60], who compared the mixing efficiency of Starlam (IMM) of different sizes.

In Figure 6.8 are plotted the ratio of the mixing time to the square of the characteristic channel dimension of the mixer versus the Reynolds number in the mixing channel for different micromixers.

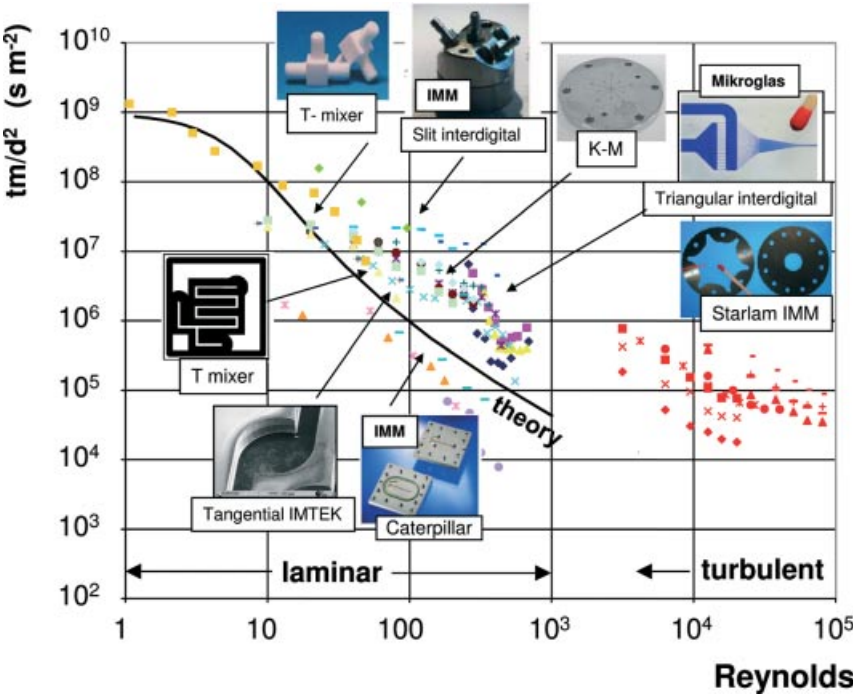

Figure 6.8 Ratio of the mixing time to the square of characteristic flow dimension versus Reynolds number. Comparison of different micromixers with theoretical Equation (6.10).

The continuous line represents the theoretical value of the (mixing time/d^2) given by Equation (6.10). At low Reynolds numbers, mixing is almost pure diffusive and t_{mixing}/d^2 is of the order of the reciprocal of the molecular diffusion coefficient in water. At higher Reynolds numbers, almost all of the values, whatever the type of mixer, lie on the same trend, in fair agreement with theory. However, there is still a certain discrepancy, which can be explained by the difficulty in properly choosing the real characteristic channel diameter in 3D mixers with complex geometries. In the same figure are plotted the experimental values of the Starlam mixers from IMM, whose values obtained in turbulent flow regimes are noticeably far from the theoretical values given by a laminar flow model.

For micromixers for which experimental pressure drop data are available, it is possible to estimate the specific power dissipation from Equation (6.4) between the inlet and the outlet pressure measurement points. It is assumed here that the estimated specific power contributes to mixing, which is a rough estimation because of the pressure drop induced by the micromixer pipe connections. In Figure 6.9 is plotted the mixing time with respect to the specific power dissipation for several mixers. The experimental mixing times scale fairly well as a power law of the

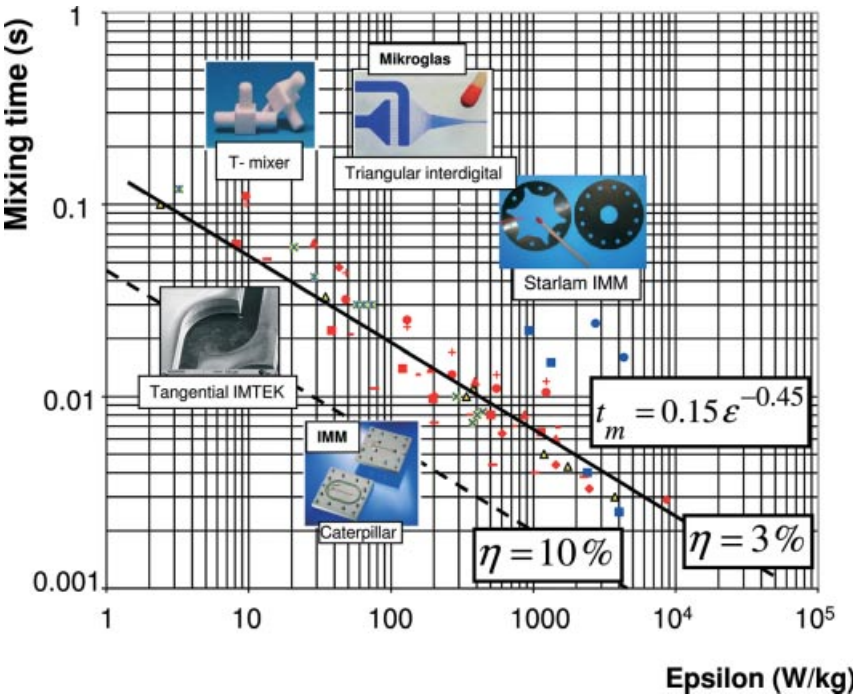

Figure 6.9 Evolution of the mixing time in different micromixers versus specific power dissipation. Influence of the energetic mixing efficiency.

dissipation with an order of −0.45, very close to the theoretical value of −0.5. Very high values of power dissipation can be obtained in micromixers, much larger than in conventional mixers in turbulent flow. The shorter mixing times which can be obtained are of the order of several milliseconds, much higher than values which could be pre-estimated from theory. In fact, the comparison of the experimental correlation with the theoretical relation presented previously led to the evaluation of the energetic efficiency of mixing as about 3%. This value is slightly larger than values obtained by Baldyga and co-workers [27] in classical mixers (1% in extruders), but not significantly different. In other respects, this result is also disappointing because whatever the internal geometry of the mixer, the power dissipation seems to be the only relevant parameter to design an efficient mixer.

In the same figure is plotted the mixing time correlation (dashed line) which would be obtained with an energetic mixing efficiency of 10%. As explained by Equation (6.13), the mixing time is almost inversely proportional to the efficiency. An increase in the energetic mixing efficiency by a factor of three (from 3 up to 10%) has the same influence on the mixing time as an increase of one decade in the power dissipation. This result shows the importance of, but also the difficulty in, properly designing internal flows in micromixers.

6.5 Conclusions

It has been shown in this chapter how to characterize mixing efficiency in micromixers and particularly how to relate mixing time to relevant operating parameters such as the Peclet number and the specific power dissipation. In spite of a low mixing energetic efficiency, micromixers can mix in a few milliseconds, much faster than conventional mixers.

However, it is not so much the importance of the intrinsic value of the mixing time but rather the possibility of improving the selectivity of the chemical reactions that is relevant.

There are mainly three characteristic features of micromixers that might be effective for the enhancement of chemical selectivity: fast mixing, efficient heat exchange (which has not been considered here) and precise residence time control, although it is difficult to separate completely the effects of these three factors on the outcome of chemical reactions.

Several studies [1, 62–65] illustrated with special emphasis the enhancement of product selectivity, so that it has become a general idea that the better the mixing is, the higher is the selectivity. If it is often true in practice, this is not always the case, and there are some reports of no improvement with using micromixers [1]; cases with unfavorable effects are unfortunately not usually reported.

In fact, it is extremely complex to predict the influence of mixing on product selectivity. This would require detailed modeling of an incompletely mixed reactor and kinetic data, difficult to obtain for multistep reactions, without any prohibitive effort. However, with knowledge of the reaction mechanism, but without the kinetics, a simple method can be applied which does not determine quantitatively the extent of a mixing effect but rather indicates qualitatively how partial segregation and feed configuration influence the rates of formation of the desired and undesired products and hence the selectivity [66, 67].

Depending on the reactions, results can be very different, and it is almost impossible to predict quantitatively the effect of improved mixing by rules of thumb. Few studies have addressed the relationship between the micromixer geometry and the product composition of multiple reactions and, in that sense, the work carried out by Aoki *et al*. [68] is pioneering and interesting, because it shows all the complexity of this topic. Even if it is undeniable that micromixers have brought considerable improvements in reactions control, one should encourage the user to be careful in the interpretation and the use of the experimental results of product selectivity.

References

1 V. Hessel, S. Hardt, H. Löwe, *Chemical Micro Process Engineering – Fundamentals, Modelling and Reactions*, 1st edn, Wiley-VCH Verlag GmbH, Weinheim, **2004**.

2 S. Wiggins, J. M. Ottino, Introduction: mixing in microfluidics, *Philos. Trans. R. Soc. London, Ser. A*, **2004**, *362*, 923–935.

3 A. E. Kamholz, *Lab Chip*, **2004**, *4*, 16N.

4 H. A. Stone, A. D. Stroock, A. Ajdari, *Annu. Rev. Fluid Mech.*, **2004**, *36*, 381.

5 N.-T. Nguyen, Z. Wu, Micromixers – a review *J. Micromech. Microeng.*, **2005**, *15*, 1–16.

6 T. M. Squires, S. R. Quake, Microfluidics: fluid physics at the nanoliter scale, *Rev. Mod. Phys.*, **2005**, *77*, 977–1026.

7 V. Hessel, H. Löwe, F. Schönfeld, Micromixers – a review on passive and active mixing principles, *Chem. Eng. Sci.*, **2005**, *60*, 2479–2501.

8 H. Li, R. Ewoldt, M. G. Olsen, Turbulent and transitional velocity measurements in a rectangular microchannel using microscopic particle image velocimetry, *Exp. Thermal Fluid Sci.*, **2005**, *29*, 435–446.

9 J. J. Ou, W. E. Ranz, Mixing and chemical reactions: a contrast between fast and slow reactions, *Chem. Eng. Sci.*, **1983**, *38*, 1005–1013.

10 J. J. Ou, W. E. Ranz, Mixing and chemical reactions: chemical selectivities, *Chem. Eng. Sci.*, **1983**, *38*, 1015–1019.

11 J. Baldyga, J. R. Bourne, Distribution of striation thickness from impingement mixers in reaction injection molding, *Polym. Eng. Sci.*, **1983**, *23*, 556–559.

12 J. Baldyga, J. R. Bourne, Mixing and fast chemical reaction VIII, *Chem. Eng. Sci.*, **1984**, *39*, 329–334.

13 I. M. Sokolov, A. Blumen, Reactions in systems with mixing, *J. Phys. A: Math. Gen.*, **1991**, *24*, 3687–3700.

14 K. T. Li, H. L. Toor, Turbulent reactive mixing with a series-parallel reaction: effect of mixing on yield, *AIChE J.*, **1986**, *32*, 1312–1320.

15 J. Baldyga, J. R. Bourne, A fluid mechanical approach to turbulent mixing and chemical reaction. Part III: computational and experimental results for the new micromixing model, *Chem. Eng. Commun.*, **1984**, *28*, 259–281.

16 J. M. Ottino, Mixing and chemical-reactions – a tutorial, *Chem. Eng. Sci*, **1994**, *49*, 4005.

17 A. D. Stroock, S. K.W. Dertinger, A. Ajdari, I. Mezic, H. A. Stone, G. M. Whitesides, Chaotic mixer for microchannels, *Science*, **2002**, *295*, 647.

18 M. R. Bringer, C. J. Gerdts, H. Song, J. D. Tice, R. F. Ismagilov, Microfluidic systems for chemical kinetics that rely on chaotic mixing in droplets, *Philos. Trans. R. Soc. London, Ser. A*, **2004**, *362*, 1087–1104.

19 S. Giona, V. Cerbelli, V. Vitacolonna, Universality and imaginary potentials in advection-diffusion equations in closed flow, *J. Fluid Mech.*, **2004**, *513*, 221.

20 P. Meunier, E. Villermaux, How vortices mix, *J. Fluid Mech.*, **2003**, *476*, 213–222.

21 J. P. Gleeson, Transient micromixing: examples of laminar and chaotic stirring, *Phys. Fluids*, **2005**, *17*, 100614.

22 F. Raynal, J. N. Gence, Energy saving in chaotic laminar mixing, *Int. J. Heat Mass Transfer*, **1997**, *40*, 3267–3273.

23 W. Gerlinger, K. Schneider, L. Falk, H. Bockhorn, Numerical simulation of the mixing of passive and reactive scalars in two-dimensional flows dominated by coherent vortices, *Chem. Eng. Sci.*, **2000**, *55*, 4255–4269.

24 E. Ott, J. Antonsen, Fractal measures of passively convected vector fields and scalar gradients in chaotic fluid flows, *Phys. Rev. A*, **1985**, *39*, 3660–3671.

25 F. Raynal, J. N. Gence, Efficient stirring in planar, time periodic laminar flows, *Chem. Eng. Sci.*, **1995**, *50*, 631–640.

26 J. M. Ottino, W. E. Ranz, C. W. Macosko, A lamellar model for analysis of liquid–liquid mixing, *Chem. Eng. Sci.*, **1979**, *34*, 877.

27 J. Baldyga, A. Rozen, F. Mostert, A model of laminar micromixing with application to parallel chemical reactions, *Chem. Eng. J.*, **1998**, *69*, 7–20.

28 J. W. Hiby, Definition and measurement of the degree of mixing in liquid mixtures, *Int. Chem. Eng.*, **1981**, *21*, 197–204.

29 R. S. Brodkey, Invited review. Fundamentals of turbulent motion, mixing and kinetics, *Chem. Eng. Commun.*, **1981**, *8*, 1–23.

30 J. W. Hiby, Definition and measurement of the degree of mixing in liquid mixtures, *Int. Chem. Eng.*, **1981**, *21*, 197–204.

31 V. Hessel, S. Hardt, H. Löwe, F. Schönfeld, Laminar mixing in different interdigital micromixers: I. Experimental characterization. *AIChE J.* **2003**, *49*, 566–577.

32 S. H. Wong, M. C. L. Ward, C. W. Wharton, Micro T-mixer as a rapid mixing micromixer, *Sens. Actuators B*, **2004**, *100*, 359–379.

33 F. Schönfeld, V. Hessel, C. Hofmann, An optimised split-and-recombine micro mixer with uniform 'chaotic' mixing. *Lab Chip*, **2004**, *4*, 65–69.

34 X. Fu, S. Liu, X. Ruan, H. Yang, Research on staggered oriented ridges static micromixers, *Sens. Actuators B*, **2006**, *114*, 618–624.

35 T. J. Johnson, D. Ross, L. E. Locascio, Rapid microfluidic mixing, *Anal. Chem.*, **2002**, *74*, 45–51.

36 M. Engler, N. Kockmann, T. Kiefer, P. Woias, Numerical and experimental investigations on liquid mixing in static micromixers, *Chem. Eng. J.*, **2004**, *101*, 315–322.

37 M. Hoffmann, M. Schülter, N. Räbiger, Experimental investigation of liquid–liquid mixing in T-shaped micromixers using μ-LIF and μ-PIV, *Chem. Eng. Sci.*, **2006**, *61*, 2968–2976.

38 J. B. Knight, A. Vishwanath, J. P. Brody, R. H. Austin, Hydrodynamic focusing on a silicon chip: mixing nanoliters in microseconds, *Phys. Rev. Lett.*, **1998**, *80*, 3863–3866.

39 R. E. Breidenthal, Structure in turbulent mixing layers and wakes using a chemical reaction, *J. Fluid Mech.*, **1981**, *109*, 1–24.

40 N. Schwesinger, T. Frank, H. Wurmus, A modular microfluidic system with an integrated micromixer, *J. Micromech. Microeng.*, **1996**, *6*, 99–102.

41 R. H. Liu, M. A. Stremler, K. V. Sharp, M. G. Olsen, J. G. Santiago, R. J. Adrian, Passive mixing in a three-dimensional serpentine microchannel, *J. Microelectromech. Syst.*, **2000**, *9*, 190–197.

42 D. S. Kim, S. W. Lee, T. H. Kwon, S. S. Lee, A barrier embedded chaotic micromixer, *J. Micromech. Microeng.*, **2004**, *14*, 798–805.

43 S. W. Lee, D. S. Kim, S. S. Lee, T. H. Kwon, A split and recombination micromixer fabricated in a PDMS three-dimensional structure, *J. Micromech. Microeng.*, **2006**, *16*, 1067–1072.

44 J. Branebjerg, B. Fabius, B. Gravesen, Application of miniature analysers: from microfluidic components to μTAS, in *Micro Total Analysis Systems*, ed. A. Van den Berg, P. Bergfeld, Kluwer, Dordrecht, **1995**, pp. 141–151.

45 S. Hardt, H. Pennemann, F. Schönfeld, Theoretical and experimental characterization of a low-Reynolds number split-and-recombine mixer, *Microfluidics Nanofluidics*, **2006**, *2*, 237–248.

46 H. Mensinger, T. Richter, V. Hessel, J. Döpper, W. Ehrfeld, Microreactor with integrated static mixer and analysis system, in *Micro Total Analysis Systems*, ed. A. Van den Berg, P. Bergfeld, Kluwer, Dordrecht, **1995**, pp. 237–234.

47 S. Ehlers, K. Elgeti, T. Menzel, G. Wiessmeier, Mixing in the offstream of a microchannel system, *Chem. Eng. Process.*, **2000**, *39*, 291–298.

48 P. Guichardon, L. Falk, Characterization of micromixing efficiency by the iodide–iodate reaction system. Part I. Experimental procedure, *Chem. Eng. Sci.*, **2000**, *55*, 4233.

49 J. J. Custer, S. Natelson, Spectrophotometric determination of micro quantities of iodine, *Anal. Chem.*, **1949**, *21*, 1005.

50 J. Baldyga, A closure model for homogenous chemical reactions, *Chem. Eng. Sci.*, **1994**, *49*, 1985–2003.

51 J. Baldyga, J. R. Bourne, Simplification of micromixing in homogeneous stirred tank reactors, *Chem. Eng. Res. Des.*, **1988**, *66*, 33.

52 M. C. Fournier, L. Falk, J. Villermaux, A new parallel competing reaction system for assessing micromixing efficiency. Determination of micromixing time by a

simple model, *Chem. Eng. Sci.*, **1996**, *51*, 5187.

53 J. Villermaux, Micromixing phenomena in stirred reactors, in *Encyclopedia of Fluid Mechanics*, Gulf Publishing, Houston, TX, **1986**, Chapter 27.

54 J. Villermaux, L. Falk, A generalized mixing model for initial contacting of reactive fluids, *Chem. Eng. Sci.*, **1994**, *49*, 5127–5140.

55 S. Panic, S. Loebbecke, T. Tuercke, J. Antes, D. Boškovic, Experimental approaches to a better understanding of mixing performance of microfluidic devices, *Chem. Eng. J.*, **2004**, *101*, 409–419.

56 N. Kockmann, T. Kiefer, M. Engler, P. Woias, Convective mixing and chemical reactions in microchannels with high flow rates, *Sens. Actuators B*, **2006**, *117*, 495–508.

57 H. Nagasawa, N. Aoki, K. Mae, Effects of channel geometry on mixing performance of micromixers using collision of fluid segments, *Chem. Eng. Technol.*, **2005**, *28*, 324–330.

58 R. Keoschkerjan, M. Richter, D. Boskovic, F. Schnürer, S. Löbbecke, Novel multifunctional microreaction unit for chemical engineering, *Chem. Eng. J.*, **2004**, *101*, 469–475.

59 M.-A. Schneider, T. Maeder, P. Ryser, F. Stoessel, A microreactor-based system for the study of fast exothermic reactions in liquid phase: characterization of the system, *Chem. Eng. J.*, **2004**, *101*, 241–250.

60 Y. Men, V. Hessel, P. Löb, H. Löwe, B. Werner, T. Baier, Determination of the segregation index to sense the mixing quality of pilot and production-scale microstructured mixers, *Trans IChemE, Part A, Chemical Engineering Research and Design*, **2007**, *85*, 605–611.

61 K. Jähnisch, V. Hessel, H. Löwe, M. Baerns, Chemistry in microstructured reactors, *Angew. Chem. Int. Ed.*, **2004**, *43*, 406–446.

62 J. Yoshida, A. Nagaki, T. Iwasaki, S. Suga, Enhancement of chemical selectivity by microreactors, *Chem. Eng. Technol.*, **2005**, *28*, 259–266.

63 S. J. Haswell, P. Watts, Green chemistry: synthesis in micro reactors, *Green Chem.* **2003**, *5*, 240–249.

64 P. Watts, S. J. Haswell, The application of micro reactors for organic synthesis, *Chem. Soc. Rev.*, **2005**, *3*, 235–246.

65 B. P. Mason, K. E. Price, J. L. Steinbacher, A. R. Bogdan, D. T. McQuade, Greener approaches to organic synthesis using microreactor technology, *ChemInform*, **2007**, *38*, 36.

66 J. R. Bourne, H. L. Toor, Simple criteria for mixing effects in complex reactions, *AIChE J.* **1977**, *23*, 602–604.

67 R. S. Brodkey, J. Lewalle, Reactor selectivity based on first-order closures of the turbulent concentration equations, *AIChE J.* **1985**, *31*, 111–118.

68 N. Aoki, S. Hasebe, K. Mae, Mixing in microreactors: effectiveness of lamination segments as a form of feed on product distribution for multiple reactions, *Chem. Eng. J.*, **2004**, *101*, 323–331.